

Field-sensitive dislocation bound states in two-dimensional d -wave altermagnets

Di Zhu,¹ Dongling Liu,¹ Zheng-Yang Zhuang,¹ Zhigang Wu,^{2,3,4} and Zhongbo Yan^{1,*}

¹Guangdong Provincial Key Laboratory of Magnetolectric Physics and Devices,
School of Physics, Sun Yat-Sen University, Guangzhou 510275, China

²Shenzhen Institute for Quantum Science and Engineering (SIQSE),
Southern University of Science and Technology, Shenzhen, P. R. China.

³International Quantum Academy, Shenzhen 518048, China.

⁴Guangdong Provincial Key Laboratory of Quantum Science and Engineering,
Southern University of Science and Technology Shenzhen, 518055, China.

(Dated: June 14, 2024)

When a two-dimensional d -wave altermagnet is grown on a substrate, the interplay of momentum-dependent spin splittings arising from altermagnetism and Rashba spin-orbit coupling gives rise to a nodal band structure with band degeneracies enforced by a $C_{4z}\mathcal{T}$ symmetry. If we break the $C_{4z}\mathcal{T}$ symmetry by an exchange field, the band degeneracies are found to be immediately lifted, leading to a topological band structure characterized by nontrivial strong and weak topological indices. Remarkably, both the strong topological index and the Z_2 -valued weak topological indices depend sensitively on the direction of the exchange field. As a consequence of the bulk-defect correspondence, we find that the unique dependence of weak topological indices on the exchange field in this system dictates that the presence or absence of topological bound states at lattice dislocations also depends sensitively on the direction of the exchange field. When the substrate is an s -wave superconductor, we find that a similar dependence of band topology on the exchange field gives rise to field-sensitive dislocation Majorana zero modes. As topological dislocation bound states are easily detectable by scanning tunneling microscopy, our findings unveil a promising experimental diagnosis of altermagnetic materials among an ever growing list of candidates.

I. INTRODUCTION

Altermagnetism (AM) has attracted increasing interest recently as a collinear magnetic order with salient properties distinct from the conventional collinear ferromagnetism and antiferromagnetism¹⁻²². In real space, the magnetic moments of an altermagnet are collinearly arranged to form a Néel order, just like an antiferromagnet. However, unlike the antiferromagnets the two sublattices with opposite magnetic moments in a magnetic unit cell of the altermagnet cannot be mapped to each other by the combined symmetry operations of time reversal and inversion/translation. Instead, they are mapped to each other by the combined symmetry operations of time reversal and rotation/mirror^{1,2}. A remarkable consequence of this difference in symmetry is that the AM leads to momentum-dependent spin-splitting electronic band structures but maintains symmetry-compensated zero net magnetization. Thus, it is not only distinct from ferromagnetism which leads to momentum-independent spin splitting and finite magnetization, but also distinguishes itself from antiferromagnetism which results in degenerate band structures. Notably, the spin splitting induced by AM can reach the order of 1eV, and the symmetry pattern of the spin splitting is rich, exemplified by the classification of AM into groups dubbed d -, g - and i -wave AM. Excitingly, several materials, including insulating MnTe²³⁻²⁶ and metallic CrSb²⁷⁻³¹, have been experimentally confirmed to be altermagnets by high-resolution angle-resolved photoemission spectroscopy (ARPES). On the theoretical front, first-principle³²⁻⁴⁰ and model⁴¹⁻⁴⁷ calculations have predicted an ever growing list of candidates for AM. Furthermore, many studies have also shown that AM can give rise to numerous interesting effects and phases, such as giant and tun-

neling magnetoresistance⁴⁸, diverse tunneling phenomena in superconductor/altermagnet junctions⁴⁹⁻⁵⁷, finite-momentum Cooper pairing⁵⁸⁻⁶⁰, unconventional superconductivity⁶¹⁻⁶⁵, various types of Hall effects⁶⁶⁻⁶⁹, and anisotropic RKKY interaction between spin impurities^{70,71}.

Because altermagnetic materials are often grown on substrates which can induce spin-orbit coupling (SOC), theoretical studies of altermagnetic materials need to also take into account this effect. SOC is known as another basic mechanism giving rise to momentum-dependent spin splitting and the interplay of AM and SOC can result in band structures of rich topological properties⁷². Thus far, the d -wave AM has been the focus of most of the theoretical studies. It has been shown that the band structure of an intrinsic d -wave altermagnet normally has spin-polarized Dirac points in two dimensions (2D), and the further presence of SOC can gap out the Dirac points and result in first-order topological insulator phases^{66,73}. Furthermore, when intrinsic superconductivity occurs in a 2D d -wave altermagnet with Rashba SOC, both first-order and second-order topological superconductivity are found to emerge⁶¹. Lastly, it has been shown that second-order topological insulators or superconductors can be obtained in hybrid systems composed of d -wave altermagnets and first-order topological insulators or superconductors⁷⁴⁻⁷⁸. In all these studies, the nontrivial momentum-space topology of the bulk bands is manifested in the presence of topological boundary states, dictated by the bulk-boundary correspondence. Interestingly, real-space topological defects, which are ubiquitous in materials and are characterized by real-space topological invariants, can also reflect the momentum-space topology in a distinct way, known as the bulk-defect correspondence⁷⁹⁻⁸¹.

The types of topological defects in materials are

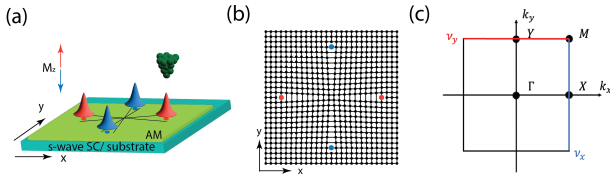


FIG. 1. (a) A schematic diagram of field-sensitive dislocation bound states and their experimental measurement by scanning tunneling microscopy. The 2D altermagnetic material grown on an insulator substrate or an s -wave superconductor has two pairs of dislocations with perpendicular Burgers vectors. The color correspondence between the bell-shaped surfaces denoting topological dislocation bound states and the arrows denoting the exchange field's direction illustrates the fact that which pair of the dislocations carries topological bound states relies on the exchange field's direction. (b) Details of the dislocation configuration. The two blue (red) dots correspond to the cores of a pair of dislocations with Burgers vector $\mathbf{B} = \pm e_x$ ($\pm e_y$). The two pairs of dislocations with perpendicular Burgers vectors form a cross-shaped defect. (c) 2D Brillouin zone. $\Gamma = (0, 0)$, $\mathbf{X} = (\pi, 0)$, $\mathbf{Y} = (0, \pi)$ and $\mathbf{M} = (\pi, \pi)$ are four high symmetry points. Two weak topological indices, ν_x and ν_y , which determine the presence or absence of topological dislocation bound states, are defined on the blue and red lines at the Brillouin zone's boundary.

diverse^{82,83}. For lattice topological defects, disclinations and dislocations are two classes that attract particular interest in the context of topological phases⁸⁴⁻⁹⁵. In the seminal work of Ran, Zhang and Vishwanath⁹⁶, it was discovered that a lattice dislocation can harbor a pair of 1D gapless helical modes in 3D topological insulators; the topological criterion for the existence of these topological dislocation modes is given by $\mathbf{B} \cdot \mathbf{M}_\nu = \pi \pmod{2\pi}$, where \mathbf{B} refers to the Burgers vector which is the real-space topological invariant characterizing the dislocation, and $\mathbf{M}_\nu = \sum_{i=1}^3 \nu_i \mathbf{G}_i / 2$. Here $\nu_i = \{0, 1\}$ is the weak topological indices defined on the high symmetry planes at the Brillouin zone's boundary⁹⁷ and \mathbf{G}_i is the reciprocal lattice vectors. \mathbf{M}_ν acts like a time-reversal invariant momentum. Later, it was demonstrated that the topological criterion can also be generalized to 2D and is applicable to topological superconductors as well⁹⁸. In 2D, when the topological criterion is fulfilled, the topological dislocation modes are 0D bound states. As an application, it was shown that the presence or absence of dislocation bound states in a 2D topological insulator with C_{4z} rotation symmetry can serve as a bulk probe to diagnose the location of band inversion⁹⁹.

In this paper, we investigate topological dislocation modes in a 2D d -wave altermagnet grown on a substrate. Because of the structure asymmetry, Rashba SOC becomes an important factor in the determination of the band structure in the altermagnet. Although the d -wave AM breaks the time-reversal symmetry (\mathcal{T}) and C_{4z} rotation symmetry, it respects their combination, the $C_{4z}\mathcal{T}$ symmetry. As the Rashba SOC also respects this symmetry, the cooperation of d -wave AM and Rashba SOC leads to a unique spin-splitting band structure with spin textures and Berry curvatures respecting this symmetry too⁶¹. Furthermore, despite the existence of spin splitting at generic momenta in the Brillouin zone, the band struc-

ture has nodal points at the two $C_{4z}\mathcal{T}$ invariant momenta. The $C_{4z}\mathcal{T}$ -symmetric band structure serves as the indication of a critical phase, since a weak perturbation breaking the $C_{4z}\mathcal{T}$ symmetry can gap out the nodal points and lead to topological gapped phases. As we are interested in these gapped phases, we consider the presence of an additional exchange field which will break the $C_{4z}\mathcal{T}$ symmetry. Remarkably, we find that both the strong topological index (Chern number) and the Z_2 -valued weak topological indices characterizing the gapped band structure depend sensitively on the exchange field's direction. As a result, whether a dislocation harbors topological bound states hinges on the exchange field's direction. Furthermore, when the substrate is an s -wave superconductor, we find that a similar dependence of band topology on the exchange field gives rise to field-sensitive dislocation Majorana zero modes.

The rest of the paper is organized as follows. In Sec.II, we describe the theoretical model and analyze the dependence of topological indices on the exchange field. By considering a cross-shaped defect consisting of two pairs of dislocations with perpendicular Burgers vectors, we illustrate that the presence of topological bound states at the dislocation cores depends sensitively on the exchange field's direction. In Sec.III, we generalize this analysis and show that field-sensitive dislocation Majorana zero modes can be obtained when the substrate is an s -wave superconductor. In Sec.IV, we discuss our findings and conclude the paper.

II. DISLOCATION BOUND STATES IN 2D METAL WITH d -WAVE AM AND RASHBA SOC

We first consider a 2D altermagnet grown on an insulator substrate and subject to a perpendicular exchange/Zee-man field, as illustrated in Fig.1(a). In this paper, we do not distinguish between Zeeman field and exchange field in terms of terminology. In the absence of defects, the tight-binding Hamiltonian is given by⁶¹ $H = \sum_{\mathbf{k}} c_{\mathbf{k}}^\dagger \mathcal{H}_0(\mathbf{k}) c_{\mathbf{k}}$ with $c_{\mathbf{k}}^\dagger = (c_{\mathbf{k},\uparrow}^\dagger, c_{\mathbf{k},\downarrow}^\dagger)$ and

$$\mathcal{H}_0(\mathbf{k}) = -2t(\cos k_x + \cos k_y)\sigma_0 + 2\lambda(\sin k_y\sigma_x - \sin k_x\sigma_y) + [2t_{\text{AM}}(\cos k_x - \cos k_y) + M_z]\sigma_z, \quad (1)$$

Here σ_i are Pauli matrices acting on the spin degrees of freedom; the first term in \mathcal{H}_0 is the kinetic energy arising from the nearest-neighbor hoppings, the second term denotes the Rashba SOC originating from structure asymmetry, and the last term accounts for the presence of two types of exchange fields, where the first momentum-dependent part (t_{AM}) is attributed to d -wave AM and the second momentum-independent part (M_z) to an external perpendicular magnetic field or a ferromagnetic insulator substrate whose magnetization is perpendicular to the plane. Throughout the lattice constant is set to unity for notational simplicity, and without loss of generality the parameters t , λ and t_{AM} are assumed to be non-negative for the convenience of discussion.

When $M_z = 0$, the Hamiltonian has the $C_{4z}\mathcal{T}$ symmetry, even though the C_{4z} rotation symmetry ($C_{4z} = e^{i\frac{\pi}{4}\sigma_z}$) and

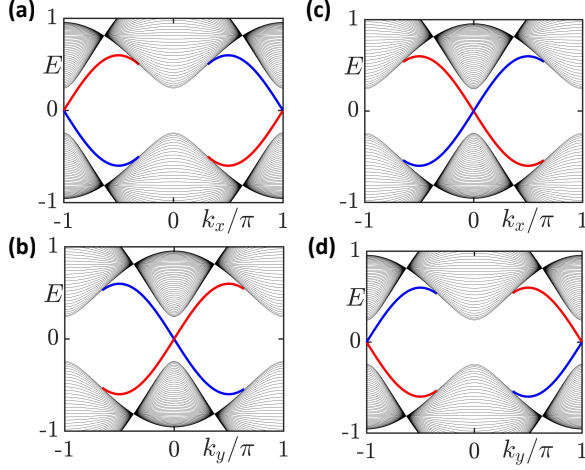


FIG. 2. Energy spectrum for a sample of ribbon geometry. For the top row, the system takes periodic (open) boundary conditions in the x (y) direction. The bottom row is just the opposite. In (a) and (b), $M_z = 0.24$, $C_- = -1$. The chiral edge state propagates clockwise on the boundary, and the edge-state spectrum crossings occur at $k_x = \pi$ and $k_y = 0$, indicating $(\nu_x, \nu_y) = (1, 0)$. In (c) and (d), $M_z = -0.24$, $C_- = 1$. The chiral edge state becomes anticlockwise, and the edge-state spectrum crossings are switched to $k_x = 0$ and $k_y = \pi$, indicating $(\nu_x, \nu_y) = (0, 1)$. The red and blue solid lines in (a) and (c) [(b) and (d)] refer to the chiral edge states on the top and bottom y -normal (left and right x -normal) edges. Common parameters are $t = 0$, $t_{AM} = 0.3$ and $\lambda = 0.3$.

time-reversal symmetry ($\mathcal{T} = -i\sigma_y\mathcal{K}$ with \mathcal{K} the complex conjugate operator) are independently broken by the d -wave AM. Because of this combined symmetry, the two energy bands have Kramers degeneracies at the two $C_{4z}\mathcal{T}$ -invariant momenta, i.e., Γ and \mathbf{M}^{G} . Once M_z becomes finite, the $C_{4z}\mathcal{T}$ symmetry is broken and the band degeneracies at Γ and \mathbf{M} are lifted, resulting in a finite energy gap between the two bands. As the system does not have time-reversal symmetry, the gapped band structure is characterized by the first-class Chern number. The Chern numbers characterizing the two bands are given by¹⁰⁰

$$C_{\pm} = \pm \frac{1}{2\pi} \int_{BZ} \frac{\mathbf{d}(\mathbf{k}) \cdot [\partial_{k_x} \mathbf{d}(\mathbf{k}) \times \partial_{k_y} \mathbf{d}(\mathbf{k})]}{2|\mathbf{d}(\mathbf{k})|^3} d^2k$$

$$= \pm \begin{cases} \text{sgn}(M_z), & 0 < |M_z| < 4t_{AM}, \\ 0, & |M_z| > 4t_{AM}. \end{cases} \quad (2)$$

where the subscript $+/-$ refers to the upper/lower band, and $\mathbf{d}(\mathbf{k}) = (2\lambda \sin k_y, -2\lambda \sin k_x, 2t_{AM}(\cos k_x - \cos k_y) + M_z)$, with the components $d_i(\mathbf{k})$ corresponding to the coefficient functions in front of the Pauli matrix σ_i in Eq. (1). The dependence of Chern number on M_z suggests that an arbitrarily weak perpendicular exchange field render the band structure topologically nontrivial. Furthermore, the Chern number has a sensitive dependence on the direction of the exchange field. Thus, a reversal of the direction of the exchange field will change the sign of the Chern number. As topological phases have bulk-boundary correspondence, it is natural to expect

that the topological boundary states will also have an intriguing dependence on the exchange field.

By calculating the energy spectrum for a sample of ribbon geometry, we find as expected that the chiral edge state reverses its chirality when the exchange field reverses its direction. What is surprising, however, is that the momentum at which the edge-state spectrum crosses undergoes a jump. When $M_z > 0$, the edge-state spectrum crossing occurs at $k_x = \pi$ on the y -normal edges [Fig.2(a)] and at $k_y = 0$ on the x -normal edges [Fig.2(b)]. Reversing the direction of the exchange field, the crossing momentum has a jump of half the reciprocal lattice vector. That is, the edge-state spectrum crossing is shifted to $k_x = 0$ on the y -normal edges [Fig.2(c)] and to $k_y = \pi$ on the x -normal edges [Fig.2(d)]. The edge-state spectrum crossing is connected to weak topological indices defined on one-dimensional lower submanifolds of the Brillouin zone, namely, the high symmetry lines of the Brillouin zone. The jump of the crossing momentum then suggests that the weak topological indices of this Hamiltonian also have a sensitive dependence on the direction of the exchange field.

The weak topological indices of interest in this work are defined on the two high symmetry lines at the boundaries of the 2D Brillouin zone, as illustrated in Fig.1(c). The two weak topological indices, labeled as ν_x and ν_y , are Z_2 -valued and their parities determine whether there is an odd number of edge-state spectrum crossings at $k_x = \pi$ and $k_y = \pi$ of the respective boundary Brillouin zone. Although the $C_{4z}\mathcal{T}$ symmetry is broken by the exchange field, the whole system still has the C_{2z} rotation symmetry described by the symmetry operator $C_{2z} = i\sigma_z$. Owing to the existence of this crystalline symmetry, the weak topological indices can be defined in terms of the eigenvalues of the C_{2z} operator at C_{2z} -invariant momenta. Following the same spirit as the Fu-Kane formula for Z_2 invariants of topological insulators⁹⁷, the explicit formulas for the two Z_2 -valued weak topological indices are given by

$$(-1)^{\nu_x} = -\xi(\mathbf{X})\xi(\mathbf{M}), \quad (-1)^{\nu_y} = -\xi(\mathbf{Y})\xi(\mathbf{M}). \quad (3)$$

where $\xi(\mathbf{k}_R)$ is the C_{2z} operator's eigenvalue for the lower-band eigenstate at the C_{2z} -invariant momentum $\mathbf{k}_R \in \{\mathbf{X}, \mathbf{Y}, \mathbf{M}\}$, i.e., $C_{2z}|u(\mathbf{k}_R)\rangle = \xi(\mathbf{k}_R)|u(\mathbf{k}_R)\rangle$. Because these eigenvalues take values of $\pm i$, a factor of “ -1 ” is introduced on the right hand side of the above equations. A straightforward calculation reveals

$$(\nu_x, \nu_y) = \begin{cases} (1, 0), & 0 < M_z < 4t_{AM}, \\ (0, 1), & -4t_{AM} < M_z < 0, \\ (0, 0), & |M_z| > 4t_{AM}. \end{cases} \quad (4)$$

The above result shows explicitly that the two weak topological indices switch their values when the exchange field in the weak-field regime ($|M_z| < 4t_{AM}$) reverses its direction. Based on the two weak topological indices, the momentum \mathbf{M}_ν reflecting the band topology is given by $\mathbf{M}_\nu = \pi(\nu_x \mathbf{e}_x + \nu_y \mathbf{e}_y)$.

Let us now consider the presence of dislocations in the system. As aforementioned, the topological criterion for the presence of topological bound states at dislocations in 2D is also

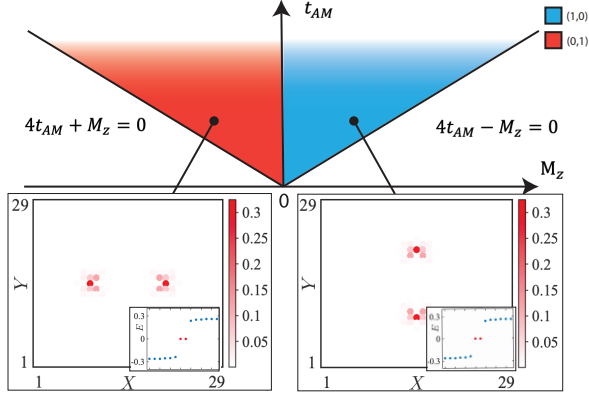


FIG. 3. Phase diagram determined via weak topological indices. The red and blue regions correspond to $(\nu_x, \nu_y) = (0, 1)$ and $(1, 0)$, respectively. The two insets below the phase diagram are energy spectra for a system with periodic boundary conditions in both x and y directions. The results show that, in the region with $(\nu_x, \nu_y) = (0, 1)$, dislocations with Burgers vector $\mathbf{B} = \pm e_y$ harbor bound states, while the ones with $\mathbf{B} = \pm e_x$ do not, and the situation is just the opposite for the region with $(\nu_x, \nu_y) = (1, 0)$. For the left (right) inset, $t_{AM} = 0.3$ and $M_z = -0.24$ (0.24). The values of other parameters are $t = 0$ and $\lambda = 0.3$.

$\mathbf{B} \cdot \mathbf{M}_\nu = \pi \pmod{2\pi}$ ⁹⁸. Because of the \mathbf{M}_ν 's sensitive dependence on the exchange field's direction, whether a dislocation with a fixed Burgers vector carries a topological bound state will thereby also sensitively depend on the exchange field's direction.

To verify this expectation, we place a cross-shaped defect consisting of two pairs of dislocations in the system [see Fig.1(b)] and numerically diagonalize the Hamiltonian under periodic boundary conditions in both x and y directions. In the case of $0 < M_z < 4t_{AM}$ for which $(\nu_x, \nu_y) = (1, 0)$, we find that the pair of dislocations with Burgers vector $\mathbf{B} = \pm e_x$ harbor topological bound states while those with Burgers vector $\mathbf{B} = \pm e_y$ do not, as shown in Fig.3. The picture is just reversed when $-4t_{AM} < M_z < 0$, demonstrating that the presence or the absence of topological bound states at a dislocation can be tuned by simply adjusting the exchange field's direction.

III. FIELD-SENSITIVE DISLOCATION MAJORANA ZERO MODES

Controllability is a desired property in the application of Majorana zero modes in topological quantum computation¹⁰¹. Following the same line of argument as before, we will show in this section that field-sensitive Majorana zero modes can also be achieved by taking advantage of the AM. To be specific, we now consider the scenario where a 2D d -wave altermagnetic metal is grown on a fully-gapped s -wave superconductor [see Fig.1(a)] and is assumed to inherit the s -wave superconductivity from the bulk superconductor though the proximity effect. Within the Bogoliubov-de Gennes (BdG) framework, the effective Hamiltonian is

given by $H = \frac{1}{2} \sum_{\mathbf{k}} \Psi_{\mathbf{k}}^\dagger \mathcal{H}_{\text{BdG}}(\mathbf{k}) \Psi_{\mathbf{k}}$, where $\Psi^\dagger(\mathbf{k}) = (c_{\mathbf{k},\uparrow}^\dagger, c_{\mathbf{k},\downarrow}^\dagger, c_{-\mathbf{k},\uparrow}, c_{-\mathbf{k},\downarrow})$ and

$$\begin{aligned} \mathcal{H}_{\text{BdG}}(\mathbf{k}) = & [-2t(\cos k_x + \cos k_y) - \mu] \tau_z \sigma_0 \\ & + [2t_{AM}(\cos k_x - \cos k_y) + M_z] \tau_z \sigma_z \\ & + 2\lambda(\sin k_y \tau_0 \sigma_x - \sin k_x \tau_z \sigma_y) + \Delta_s \tau_y \sigma_y \end{aligned} \quad (5)$$

Here μ is the chemical potential, Δ_s is the proximity-induced s -wave pairing amplitude and the new set of Pauli matrices τ_i acts on the particle-hole degrees of freedom.

We again first focus on the band topology of the BdG Hamiltonian. Since the s -wave pairing does not break the time-reversal symmetry and C_{4z} rotation symmetry, the BdG Hamiltonian also respects the $C_{4z}\mathcal{T}$ symmetry when $M_z = 0$. In a previous work, we have shown that the $C_{4z}\mathcal{T}$ symmetry forbids a 2D gapped superconductor to have a nonzero Chern number⁶¹. Despite the absence of strong topology characterized by the Chern number, weak topology is compatible with this symmetry and can be nontrivial when the system's parameters fulfill certain conditions⁷⁴. To see this, we again make use of the eigenvalues of the C_{2z} operator, which is now given by $C_{2z} = -i\tau_z \sigma_z$ due to the inclusion of particle-hole degrees of freedom. More specifically, we define

$$\begin{aligned} (-1)^{\nu_x} &= (-1)^N \prod_{n=1}^N \xi_n(\mathbf{X}) \xi_n(\mathbf{M}), \\ (-1)^{\nu_y} &= (-1)^N \prod_{n=1}^N \xi_n(\mathbf{Y}) \xi_n(\mathbf{M}), \end{aligned} \quad (6)$$

where $N = 2$ denotes the number of bands below $E = 0$, n is the band index with $E_n < 0$, and $\xi_n(\mathbf{k}_R)$ is the C_{2z} operator's eigenvalue for the negative-energy eigenstate at $\mathbf{k}_R \in \{\mathbf{X}, \mathbf{Y}, \mathbf{M}\}$, i.e., $C_{2z}|u_n(\mathbf{k}_R)\rangle = \xi_n(\mathbf{k}_R)|u_n(\mathbf{k}_R)\rangle$. A straightforward calculation yields the weak topological indices at $M_z = 0$,

$$(\nu_x, \nu_y) = \begin{cases} (1, 1), & 4t_{AM} > \sqrt{\mu^2 + \Delta_s^2}, \\ (0, 0), & 4t_{AM} < \sqrt{\mu^2 + \Delta_s^2}. \end{cases} \quad (7)$$

This result indicates that, despite the impossibility of chiral Majorana modes when $M_z = 0$, Majorana zero modes can be created at dislocations with Burgers vectors equal to either $\pm e_x$ or $\pm e_y$. Before explicitly showing this, we first complete the analysis of the bulk topology when $M_z \neq 0$.

Similar to the previous nonsuperconducting case, a finite M_z breaks the $C_{4z}\mathcal{T}$ symmetry and can induce topological superconducting phases characterized by nonzero Chern numbers. The topological phase diagram can be easily determined since the change of Chern number is associated with the close of bulk energy gap¹⁰², which takes place when $M_z = \{\pm\sqrt{(4t \pm \mu)^2 + \Delta_s^2}, \pm 4t_{AM} \pm \sqrt{\mu^2 + \Delta_s^2}\}$. Here we are not interested in determining the complete phase diagram. Rather, we are interested in the region where the exchange field is weak, i.e., when M_z is comparable to Δ_s , and when the chemical potential is close to the critical points between the weak topological superconductor and trivial superconductors, i.e., when μ is close to $\mu_{c,\pm} = \pm\sqrt{16t_{AM}^2 - \Delta_s^2}$.

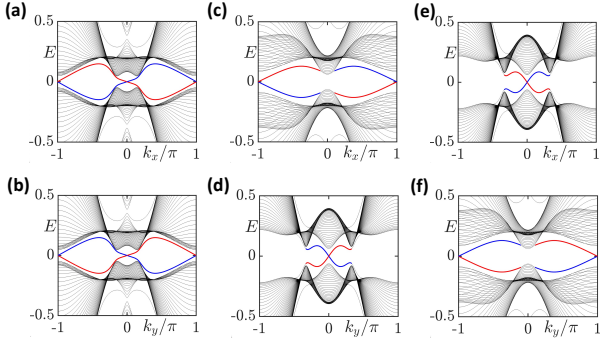


FIG. 4. BdG energy spectrum for a sample of ribbon geometry. The system takes open boundary directions in the y (x) direction and periodic boundary conditions in the x (y) direction for the top (bottom) row. In (a) and (b), $M_z = 0$, $C = 0$, and the locations of edge-state spectrum crossings suggest $(\nu_x, \nu_y) = (1, 1)$. In (c) and (d), $M_z = -0.3$, $C = -1$, and the locations of edge-state spectrum crossings suggest $(\nu_x, \nu_y) = (1, 0)$. In (e) and (f), $M_z = 0.3$, $C = 1$, and the locations of edge-state spectrum crossings suggest $(\nu_x, \nu_y) = (0, 1)$. Common parameters are $t = 0.2$, $t_{AM} = 0.3$, $\lambda = 0.3$, $\Delta_s = 0.2$, and $\mu = -1.1$.

Without loss of generality, we take $\mu = \mu_{c,-} + \delta$ where δ is a small real positive constant. Then, increasing the exchange field's strength from zero, the energy gap closes at \mathbf{X} when $M_z = 4t_{AM} - \sqrt{\mu^2 + \Delta_s^2} \simeq \delta$ (assuming $\Delta_s \ll t_{AM}$), and at \mathbf{Y} when $M_z = -4t_{AM} + \sqrt{\mu^2 + \Delta_s^2} \simeq -\delta$. The close of energy gap at \mathbf{X} changes the total Chern number of the bands below $E = 0$ from $C = 0$ to $C = 1$, and the weak topological indices (ν_x, ν_y) from $(1, 1)$ to $(0, 1)$. In contrast, the close of energy gap at \mathbf{Y} changes the total Chern number of the bands below $E = 0$ from $C = 0$ to $C = -1$, and the weak topological indices (ν_x, ν_y) from $(1, 1)$ to $(1, 0)$.

In Fig.4, we show the energy spectrum for a sample of ribbon geometry. In Figs.4(a) and 4(b), we see that there are two counter-propagating gapless states on one edge and the edge-state spectrum crossing occurs at time-reversal invariant momenta on both x -normal and y -normal edges; this is consistent with $C = 0$ and $(\nu_x, \nu_y) = (1, 1)$ for $M_z = 0$ and $4t_{AM} > \sqrt{\mu^2 + \Delta_s^2}$. In Figs.4(c) and 4(d), the number of chiral edge states and the locations of edge-state spectrum crossings suggest that $C = -1$ and $(\nu_x, \nu_y) = (1, 0)$, which is also consistent with the values as analyzed above. In Figs.4(e) and 4(f), the results show that a reversal of the exchange field's direction reverses the chirality of the gapless edge state, and leads to a switching of the locations of edge-state spectrum crossings on the x -normal and y -normal edges. This again agrees with the sign change of the Chern number and the switching of the values of ν_x and ν_y accompanying this process.

Placing a cross-shaped defect in the superconducting system and diagonalizing the Hamiltonian under periodic boundary conditions in both directions, we find the presence of Majorana zero modes at dislocations when the topological criterion $\mathbf{B} \cdot \mathbf{G}_\nu = \pi \pmod{2\pi}$ is fulfilled. To be specific, when the system is a weak topological superconductor with

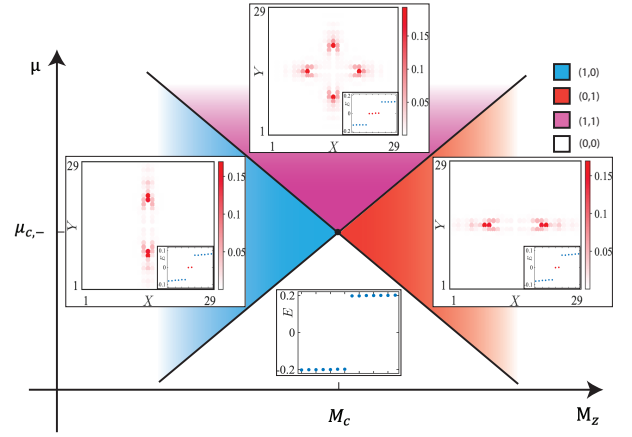


FIG. 5. Phase diagram around the critical point with $\mu_{c,-} = -\sqrt{16t_{AM}^2 - \Delta_s^2}$ and $M_c = 0$. The phase boundaries are given by $M_z = \pm(4t_{AM} - \sqrt{\mu^2 + \Delta_s^2})$. The weak topological indices (ν_x, ν_y) in the blue, white, red and purple regions take values of $(1, 0)$, $(0, 0)$, $(0, 1)$ and $(1, 1)$, respectively. The four insets at the corresponding regions show the number and distributions of Majorana zero modes at the two pairs of dislocations with $\mathbf{B} = \pm e_x$ and $\pm e_y$. The corresponding parameters of the insets on the left, right, top and bottom are $(\mu, M_z) = (-1.183, -0.3)$, $(\mu, M_z) = (-1.183, 0.3)$, $(\mu, M_z) = (-0.6, 0)$ and $(\mu, M_z) = (-1.4, 0)$. Common parameters are $t = 0.2$, $t_{AM} = 0.3$, $\lambda = 0.3$ and $\Delta_s = 0.2$.

$(\nu_x, \nu_y) = (1, 1)$ (indicated by the purple region of Fig.5), we find that there are four Majorana zero modes with their wave functions localized at the cores of the dislocations, as shown in the inset on top of the purple region. The result suggests that dislocations with Burgers vector $\mathbf{B} = \pm e_x$ and $\pm e_y$ all harbor Majorana zero modes at their cores, which agrees with the topological criterion. In comparison, when ν_x (ν_y) is trivialized by the exchange field, the two Majorana zero modes at the dislocations with $\mathbf{B} = \pm e_x$ ($\pm e_y$) disappear, while the two Majorana zero modes at the dislocations with $\mathbf{B} = \pm e_y$ ($\pm e_x$) remain intact; this is clearly shown in the inset on top of the red (blue) region in Fig.5. We can draw an important conclusion from Fig.5. Namely, when the chemical potential is close to $\mu_{c,-}$, tuning the direction of a weak exchange field can control the presence or absence of Majorana zero modes at a dislocation. These results suggest that the unique spin-splitting band structure induced by AM and Rashba SOC provides a basis for the realization of controllable Majorana modes.

IV. DISCUSSIONS AND CONCLUSIONS

The combination of d -wave AM and Rashba SOC leads to a unique spin-splitting band structure respecting the $C_{4z}\mathcal{T}$ symmetry. Breaking the $C_{4z}\mathcal{T}$ symmetry by an exchange field, we find that both the strong topology and the weak topology of the resulting band structure show a sensitive dependence on the exchange field's direction. As a consequence of the sensitive dependence of weak topological indices on the ex-

change field's direction, we find that the presence or absence of topological bound states at a dislocation can be easily controlled by adjusting the exchange field's direction. By putting the 2D altermagnetic metal in proximity to an s -wave superconductor, we find a similar sensitive dependence of the band topology and dislocation bound states on the exchange field when the chemical potential is appropriately chosen. As the dislocation bound states are Majorana zero modes in this case, their sensitivity towards external fields implies high degrees of controllability; this may make the superconducting altermagnetic materials stand out as platforms to detect and manipulate Majorana zero modes.

From a symmetry perspective, the change from one set of topological dislocation bound states into their C_{4z} -rotational counterparts upon reversing the exchange field's direction is a direct manifestation of the $C_{4z}\mathcal{T}$ symmetry of the pristine altermagnetic system. In the light of this, an observation of this switching behavior of topological dislocation bound states can be taken as a strong signature of d -wave AM. In experiments, the field-sensitive dislocation bound states are robust due to

their topological origin and can be easily detected by scanning tunneling microscopy. Given the ubiquitous presence of topological defects in real materials and a continuously accumulated list of candidates for altermagnetic materials, our findings unveil a promising route to an effective experimental diagnosis of AM in these materials.

ACKNOWLEDGEMENTS

D. Z., D. L., Z.-Y. Z, and Z. Y. are supported by the National Natural Science Foundation of China (Grant No. 12174455), Natural Science Foundation of Guangdong Province (Grant No. 2021B1515020026), and Guangdong Basic and Applied Basic Research Foundation (Grant No. 2023B1515040023). Z. W. is supported by National Key R&D Program of China (Grant No. 2022YFA1404103), NSFC (Grant No. 11974161) and Shenzhen Science and Technology Program (Grant No. KQTD20200820113010023).

* yanzhb5@mail.sysu.edu.cn

¹ Libor Šmejkal, Jairo Sinova, and Tomas Jungwirth, "Beyond Conventional Ferromagnetism and Antiferromagnetism: A Phase with Nonrelativistic Spin and Crystal Rotation Symmetry," *Phys. Rev. X* **12**, 031042 (2022).

² Libor Šmejkal, Jairo Sinova, and Tomas Jungwirth, "Emerging Research Landscape of Altermagnetism," *Phys. Rev. X* **12**, 040501 (2022).

³ Libor Šmejkal, Rafael González-Hernández, T. Jungwirth, and J. Sinova, "Crystal time-reversal symmetry breaking and spontaneous Hall effect in collinear antiferromagnets," *Science Advances* **6**, eaaz8809 (2020).

⁴ Satoru Hayami, Yuki Yanagi, and Hiroaki Kusunose, "Momentum-dependent spin splitting by collinear antiferromagnetic ordering," *Journal of the Physical Society of Japan* **88**, 123702 (2019).

⁵ Satoru Hayami, Yuki Yanagi, and Hiroaki Kusunose, "Bottom-up design of spin-split and reshaped electronic band structures in antiferromagnets without spin-orbit coupling: Procedure on the basis of augmented multipoles," *Phys. Rev. B* **102**, 144441 (2020).

⁶ Lin-Ding Yuan, Zhi Wang, Jun-Wei Luo, Emmanuel I. Rashba, and Alex Zunger, "Giant momentum-dependent spin splitting in centrosymmetric low- Z antiferromagnets," *Phys. Rev. B* **102**, 014422 (2020).

⁷ Lin-Ding Yuan, Zhi Wang, Jun-Wei Luo, and Alex Zunger, "Prediction of low- Z collinear and noncollinear antiferromagnetic compounds having momentum-dependent spin splitting even without spin-orbit coupling," *Phys. Rev. Mater.* **5**, 014409 (2021).

⁸ Igor I. Mazin, Klaus Koepernik, Michelle D. Johannes, Rafael González-Hernández, and Libor Šmejkal, "Prediction of unconventional magnetism in doped FeSb₂," *Proceedings of the National Academy of Sciences* **118**, e2108924118 (2021).

⁹ Ding-Fu Shao, Shu-Hui Zhang, Ming Li, Chang-Beom Eom, and Evgeny Y. Tsymbal, "Spin-neutral currents for spintronics," *Nature Communications* **12**, 7061 (2021).

¹⁰ Hai-Yang Ma, Mengli Hu, Nana Li, Jianpeng Liu, Wang Yao, Jin-Feng Jia, and Junwei Liu, "Multifunctional antiferromagnetic materials with giant piezomagnetism and noncollinear spin current," *Nature Communications* **12**, 2846 (2021).

¹¹ Pengfei Liu, Jiayu Li, Jingzhi Han, Xiangang Wan, and Qihang Liu, "Spin-group symmetry in magnetic materials with negligible spin-orbit coupling," *Phys. Rev. X* **12**, 021016 (2022).

¹² Zexin Feng, Xiaorong Zhou, Libor Šmejkal, Lei Wu, Zengwei Zhu, Huixin Guo, Rafael González-Hernández, Xiaoning Wang, Han Yan, Peixin Qin, Xin Zhang, Haojiang Wu, Hongyu Chen, Ziang Meng, Li Liu, Zhengcai Xia, Jairo Sinova, Tomáš Jungwirth, and Zhiqi Liu, "An anomalous Hall effect in altermagnetic ruthenium dioxide," *Nature Electronics* **5**, 735–743 (2022).

¹³ R. D. Gonzalez Betancourt, J. Zubáč, R. Gonzalez-Hernandez, K. Geishendorf, Z. Šobán, G. Springholz, K. Olejník, L. Šmejkal, J. Sinova, T. Jungwirth, S. T. B. Goennenwein, A. Thomas, H. Reichlová, J. Železný, and D. Kriegner, "Spontaneous Anomalous Hall Effect Arising from an Unconventional Compensated Magnetic Phase in a Semiconductor," *Phys. Rev. Lett.* **130**, 036702 (2023).

¹⁴ I. I. Mazin, "Altermagnetism in MnTe: Origin, predicted manifestations, and routes to detwinning," *Phys. Rev. B* **107**, L100418 (2023).

¹⁵ Ilja Turek, "Altermagnetism and magnetic groups with pseudoscalar electron spin," *Phys. Rev. B* **106**, 094432 (2022).

¹⁶ A. Hariki, T. Yamaguchi, D. Kriegner, K. W. Edmonds, P. Wadley, S. S. Dhesi, G. Springholz, L. Šmejkal, K. Výborný, T. Jungwirth, and J. Kuneš, "X-ray Magnetic Circular Dichroism in Altermagnetic α -MnTe," *arXiv e-prints*, arXiv:2305.03588 (2023), arXiv:2305.03588 [cond-mat.mtrl-sci].

¹⁷ Sayantika Bhowal and Nicola A. Spaldin, "Ferrocally Ordered Magnetic Octupoles in d -Wave Altermagnets," *Phys. Rev. X* **14**, 011019 (2024).

¹⁸ Xiaodong Zhou, Wanxiang Feng, Run-Wu Zhang, Libor Šmejkal, Jairo Sinova, Yuriy Mokrousov, and Yugui Yao, "Crystal Thermal Transport in Altermagnetic RuO₂," *Phys. Rev. Lett.* **132**, 056701 (2024).

- ¹⁹ Lei Han, Xizhi Fu, Rui Peng, Xingkai Cheng, Jiankun Dai, Liangyang Liu, Yidian Li, Yichi Zhang, Wenxuan Zhu, Hua Bai, Yongjian Zhou, Shixuan Liang, Chong Chen, Qian Wang, Xianzhe Chen, Luyi Yang, Yang Zhang, Cheng Song, Junwei Liu, and Feng Pan, “Electrical 180° switching of Néel vector in spin-splitting antiferromagnet,” *Science Advances* **10**, eadn0479 (2024).
- ²⁰ Xiaobing Chen, Jun Ren, Yanzhou Zhu, Yutong Yu, Ao Zhang, Pengfei Liu, Jiayu Li, Yuntian Liu, Caiheng Li, and Qihang Liu, “Enumeration and representation theory of spin space groups,” arXiv e-prints , arXiv:2307.10369 (2023), arXiv:2307.10369 [cond-mat.mtrl-sci].
- ²¹ Zhenyu Xiao, Jianzhou Zhao, Yanqi Li, Ryuichi Shindou, and Zhi-Da Song, “Spin Space Groups: Full Classification and Applications,” arXiv e-prints , arXiv:2307.10364 (2023), arXiv:2307.10364 [cond-mat.mes-hall].
- ²² Yi Jiang, Ziyin Song, Tiannian Zhu, Zhong Fang, Hongming Weng, Zheng-Xin Liu, Jian Yang, and Chen Fang, “Enumeration of spin-space groups: Towards a complete description of symmetries of magnetic orders,” arXiv e-prints , arXiv:2307.10371 (2023), arXiv:2307.10371 [cond-mat.mtrl-sci].
- ²³ T. Osumi, S. Souma, T. Aoyama, K. Yamauchi, A. Honma, K. Nakayama, T. Takahashi, K. Ohgushi, and T. Sato, “Observation of a giant band splitting in altermagnetic MnTe,” *Phys. Rev. B* **109**, 115102 (2024).
- ²⁴ Suyoung Lee, Sangjae Lee, Saegyeol Jung, Jiwon Jung, Donghan Kim, Yeonjae Lee, Byeongjun Seok, Jaeyoung Kim, Byeong Gyu Park, Libor Šmejkal, Chang-Jong Kang, and Changyoung Kim, “Broken Kramers Degeneracy in Altermagnetic MnTe,” *Phys. Rev. Lett.* **132**, 036702 (2024).
- ²⁵ J. Krempaský, L. Šmejkal, S. W. D’Souza, M. Hajlaoui, G. Springholz, K. Uhlířová, F. Alarab, P. C. Constantinou, V. Strocov, D. Usanov, W. R. Pudielko, R. González-Hernández, A. Birk Hellenes, Z. Jansa, H. Reichlová, Z. Šobáň, R. D. Gonzalez Betancourt, P. Wadley, J. Sinova, D. Kriegner, J. Minár, J. H. Dil, and T. Jungwirth, “Altermagnetic lifting of Kramers spin degeneracy,” *Nature* **626**, 517–522 (2024).
- ²⁶ M. Hajlaoui, S. W. D’Souza, L. Šmejkal, D. Kriegner, G. Krizman, T. Zakusylo, N. Olszowska, O. Caha, J. Michalička, A. Marmodoro, K. Výborný, A. Ernst, M. Cinchetti, J. Minar, T. Jungwirth, and G. Springholz, “Temperature dependence of relativistic valence band splitting induced by an altermagnetic phase transition,” arXiv e-prints , arXiv:2401.09187 (2024), arXiv:2401.09187 [cond-mat.mtrl-sci].
- ²⁷ Sonka Reimers, Lukas Odenbreit, Libor Šmejkal, Vladimir N. Strocov, Procopios Constantinou, Anna B. Hellenes, Rodrigo Jaeschke Ubierno, Warley H. Campos, Venkata K. Bharadwaj, Atasi Chakraborty, Thibaud Denneulin, Wen Shi, Rafal E. Dunin-Borkowski, Suvadip Das, Mathias Kläui, Jairo Sinova, and Martin Jourdan, “Direct observation of altermagnetic band splitting in CrSb thin films,” *Nature Communications* **15**, 2116 (2024).
- ²⁸ Jianyang Ding, Zhicheng Jiang, Xiuhua Chen, Zicheng Tao, Zhengtai Liu, Jishan Liu, Tongrui Li, Jiayu Liu, Yichen Yang, Runfeng Zhang, Liwei Deng, Wenchuan Jing, Yu Huang, Yuming Shi, Shan Qiao, Yilin Wang, Yanfeng Guo, Donglai Feng, and Dawei Shen, “Large band-splitting in g -wave type altermagnet CrSb,” arXiv e-prints , arXiv:2405.12687 (2024), arXiv:2405.12687 [cond-mat.mtrl-sci].
- ²⁹ Guowei Yang, Zhanghuan Li, Sai Yang, Jiyuan Li, Hao Zheng, Weifan Zhu, Saizheng Cao, Wenxuan Zhao, Jiawen Zhang, Mao Ye, Yu Song, Lun-Hui Hu, Lexian Yang, Ming Shi, Huiqiu Yuan, Yongjun Zhang, Yuanfeng Xu, and Yang Liu, “Three-dimensional mapping and electronic origin of large altermagnetic splitting near Fermi level in CrSb,” arXiv e-prints , arXiv:2405.12575 (2024), arXiv:2405.12575 [cond-mat.mtrl-sci].
- ³⁰ Meng Zeng, Ming-Yuan Zhu, Yu-Peng Zhu, Xiang-Rui Liu, Xiao-Ming Ma, Yu-Jie Hao, Pengfei Liu, Gexing Qu, Yichen Yang, Zhicheng Jiang, Kohei Yamagami, Masashi Arita, Xiaoqian Zhang, Tian-Hao Shao, Yue Dai, Kenya Shimada, Zhengtai Liu, Mao Ye, Yaobo Huang, Qihang Liu, and Chang Liu, “Observation of Spin Splitting in Room-Temperature Metallic Antiferromagnet CrSb,” arXiv e-prints , arXiv:2405.12679 (2024), arXiv:2405.12679 [cond-mat.mtrl-sci].
- ³¹ Cong Li, Mengli Hu, Zhilin Li, Yang Wang, Wanyu Chen, Balasubramanian Thiagarajan, Mats Leandersson, Craig Polley, Timur Kim, Hui Liu, Cosma Fulga, Maia G. Vergniory, Oleg Janson, Oscar Tjernberg, and Jeroen van den Brink, “Topological Weyl Altermagnetism in CrSb,” arXiv e-prints , arXiv:2405.14777 (2024), arXiv:2405.14777 [cond-mat.mtrl-sci].
- ³² Peng-Jie Guo, Yuhao Gu, Ze-Feng Gao, and Zhong-Yi Lu, “Altermagnetic ferroelectric LiFe₂F₆ and spin-triplet excitonic insulator phase,” arXiv e-prints , arXiv:2312.13911 (2023), arXiv:2312.13911 [cond-mat.mtrl-sci].
- ³³ Ze-Feng Gao, Shuai Qu, Bocheng Zeng, Yang Liu, Ji-Rong Wen, Hao Sun, Peng-Jie Guo, and Zhong-Yi Lu, “AI-accelerated Discovery of Altermagnetic Materials,” arXiv e-prints , arXiv:2311.04418 (2023), arXiv:2311.04418 [cond-mat.mtrl-sci].
- ³⁴ Shuai Qu, Ze-Feng Gao, Hao Sun, Kai Liu, Peng-Jie Guo, and Zhong-Yi Lu, “Extremely strong spin-orbit coupling effect in light element altermagnetic materials,” arXiv e-prints , arXiv:2401.11065 (2024), arXiv:2401.11065 [cond-mat.mtrl-sci].
- ³⁵ Joachim Sødequist and Thomas Olsen, “Two-dimensional altermagnets from high throughput computational screening: Symmetry requirements, chiral magnons, and spin-orbit effects,” *Applied Physics Letters* **124**, 182409 (2024), arXiv:2401.05992 [cond-mat.mtrl-sci].
- ³⁶ F. Bernardini, M. Fiebig, and A. Cano, “Ruddlesden-Popper and perovskite phases as a material platform for altermagnetism,” arXiv e-prints , arXiv:2401.12910 (2024), arXiv:2401.12910 [cond-mat.mtrl-sci].
- ³⁷ Sajjan Sheoran and Saswata Bhattacharya, “Nonrelativistic spin splittings and altermagnetism in twisted bilayers of centrosymmetric antiferromagnets,” *Physical Review Materials* **8**, L051401 (2024), arXiv:2310.19395 [cond-mat.mtrl-sci].
- ³⁸ Marko Milivojević, Marko Orozović, Silvia Picozzi, Martin Gmitra, and Srdjan Stavić, “Interplay of altermagnetism and weak ferromagnetism in two-dimensional RuF₄,” arXiv e-prints , arXiv:2401.15424 (2024), arXiv:2401.15424 [cond-mat.mtrl-sci].
- ³⁹ Sike Zeng and Yu-Jun Zhao, “The description of two-dimensional altermagnetism,” arXiv e-prints , arXiv:2405.03557 (2024), arXiv:2405.03557 [cond-mat.mtrl-sci].
- ⁴⁰ Yichen Liu, Junxi Yu, and Cheng-Cheng Liu, “Twisted Magnetic Van der Waals Bilayers: An Ideal Platform for Altermagnetism,” arXiv e-prints , arXiv:2404.17146 (2024), arXiv:2404.17146 [cond-mat.mtrl-sci].
- ⁴¹ Valentin Leeb, Alexander Mook, Libor Šmejkal, and Johannes Knolle, “Spontaneous Formation of Altermagnetism from Orbital Ordering,” *Phys. Rev. Lett.* **132**, 236701 (2024).
- ⁴² Purnendu Das, Valentin Leeb, Johannes Knolle, and Michael Knap, “Realizing Altermagnetism in Fermi-Hubbard Models with Ultracold Atoms,” arXiv e-prints , arXiv:2312.10151 (2023), arXiv:2312.10151 [cond-mat.quant-gas].

- ⁴³ Toshihiro Sato, Sonia Haddad, Ion Cosma Fulga, Fakher F. Asaad, and Jeroen van den Brink, “Altermagnetic anomalous Hall effect emerging from electronic correlations,” arXiv e-prints , arXiv:2312.16290 (2023), arXiv:2312.16290 [cond-mat.str-el].
- ⁴⁴ Mercè Roig, Andreas Kreisler, Yue Yu, Brian M. Andersen, and Daniel F. Agterberg, “Minimal Models for Altermagnetism,” arXiv e-prints , arXiv:2402.15616 (2024), arXiv:2402.15616 [cond-mat.str-el].
- ⁴⁵ Pedro M. Cónsoli and Matthias Vojta, “SU(3) altermagnetism: Lattice models, chiral magnons, and flavor-split bands,” arXiv e-prints , arXiv:2402.18629 (2024), arXiv:2402.18629 [cond-mat.str-el].
- ⁴⁶ Yue Yu, Han-Gyeol Suh, Mercè Roig, and Daniel F. Agterberg, “Altermagnetism from coincident Van Hove singularities: application to κ -Cl,” arXiv e-prints , arXiv:2402.05180 (2024), arXiv:2402.05180 [cond-mat.str-el].
- ⁴⁷ Anjishnu Bose, Samuel Vadrnais, and Arun Paramekanti, “Altermagnetism and superconductivity in a multiorbital t-J model,” arXiv e-prints , arXiv:2403.17050 (2024), arXiv:2403.17050 [cond-mat.str-el].
- ⁴⁸ Libor Šmejkal, Anna Birk Hellenes, Rafael González-Hernández, Jairo Sinova, and Tomas Jungwirth, “Giant and Tunneling Magnetoresistance in Unconventional Collinear Antiferromagnets with Nonrelativistic Spin-Momentum Coupling,” *Phys. Rev. X* **12**, 011028 (2022).
- ⁴⁹ Jabir Ali Ouassou, Arne Brataas, and Jacob Linder, “dc Josephson Effect in Altermagnets,” *Phys. Rev. Lett.* **131**, 076003 (2023).
- ⁵⁰ Chi Sun, Arne Brataas, and Jacob Linder, “Andreev reflection in altermagnets,” *Phys. Rev. B* **108**, 054511 (2023).
- ⁵¹ Michał Papaj, “Andreev reflection at the altermagnet-superconductor interface,” *Phys. Rev. B* **108**, L060508 (2023).
- ⁵² C. W. J. Beenakker and T. Vakhel, “Phase-shifted Andreev levels in an altermagnet Josephson junction,” *Phys. Rev. B* **108**, 075425 (2023).
- ⁵³ Qiang Cheng and Qing-Feng Sun, “Orientation-dependent Josephson effect in spin-singlet superconductor/altermagnet/spin-triplet superconductor junctions,” *Phys. Rev. B* **109**, 024517 (2024).
- ⁵⁴ Yutaro Nagae, Andreas P. Schnyder, and Satoshi Ikegaya, “Spin-polarized Specular Andreev Reflections in Altermagnets,” arXiv e-prints , arXiv:2403.07117 (2024), arXiv:2403.07117 [cond-mat.supr-con].
- ⁵⁵ Hans Glöckner Gil, Bjørnulf Brekke, Jacob Linder, and Arne Brataas, “Quasiclassical theory of superconducting spin-splitter effects and spin-filtering via altermagnets,” arXiv e-prints , arXiv:2403.04851 (2024), arXiv:2403.04851 [cond-mat.supr-con].
- ⁵⁶ Sachchidanand Das and Abhiram Soori, “Crossed Andreev reflection in altermagnets,” arXiv e-prints , arXiv:2402.08263 (2024), arXiv:2402.08263 [cond-mat.mes-hall].
- ⁵⁷ Bo Lu, Kazuki Maeda, Hiroyuki Ito, Keiji Yada, and Yukio Tanaka, “ φ Josephson junction induced by altermagnetism,” arXiv e-prints , arXiv:2405.10656 (2024), arXiv:2405.10656 [cond-mat.supr-con].
- ⁵⁸ Song-Bo Zhang, Lun-Hui Hu, and Titus Neupert, “Finite-momentum Cooper pairing in proximitized altermagnets,” *Nature Communications* **15**, 1801 (2024).
- ⁵⁹ Shuntaro Sumita, Makoto Naka, and Hitoshi Seo, “Fulde-Ferrell-Larkin-Ovchinnikov state induced by antiferromagnetic order in κ -type organic conductors,” *Phys. Rev. Res.* **5**, 043171 (2023).
- ⁶⁰ Debmalya Chakraborty and Annica M. Black-Schaffer, “Zero-field finite-momentum and field-induced superconductivity in altermagnets,” arXiv e-prints , arXiv:2309.14427 (2023), arXiv:2309.14427 [cond-mat.supr-con].
- ⁶¹ Di Zhu, Zheng-Yang Zhuang, Zhigang Wu, and Zhongbo Yan, “Topological superconductivity in two-dimensional altermagnetic metals,” *Phys. Rev. B* **108**, 184505 (2023).
- ⁶² Miaomiao Wei, Longjun Xiang, Fuming Xu, Lei Zhang, Gaomin Tang, and Jian Wang, “Gapless superconducting state and mirage gap in altermagnets,” *Phys. Rev. B* **109**, L201404 (2024).
- ⁶³ Bjørnulf Brekke, Arne Brataas, and Asle Sudbø, “Two-dimensional altermagnets: Superconductivity in a minimal microscopic model,” *Phys. Rev. B* **108**, 224421 (2023).
- ⁶⁴ Kristian Mæland, Bjørnulf Brekke, and Asle Sudbø, “Many-body effects on superconductivity mediated by double-magnon processes in altermagnets,” *Phys. Rev. B* **109**, 134515 (2024).
- ⁶⁵ Simran Chourasia, Aleksandr Svetogorov, Akashdeep Kamra, and Wolfgang Belzig, “Thermodynamic properties of a superconductor interfaced with an altermagnet,” arXiv e-prints , arXiv:2403.10456 (2024), arXiv:2403.10456 [cond-mat.supr-con].
- ⁶⁶ Kirill Parshukov, Raymond Wiedmann, and Andreas P. Schnyder, “Topological responses from gapped Weyl points in 2D altermagnets,” arXiv e-prints , arXiv:2403.09520 (2024), arXiv:2403.09520 [cond-mat.mes-hall].
- ⁶⁷ Yuan Fang, Jennifer Cano, and Sayed Ali Akbar Ghorashi, “Quantum geometry induced nonlinear transport in altermagnets,” arXiv e-prints , arXiv:2310.11489 (2023), arXiv:2310.11489 [cond-mat.mes-hall].
- ⁶⁸ Lotan Attias, Alex Levchenko, and Maxim Khodas, “Intrinsic anomalous and crystal Hall effects in altermagnets,” arXiv e-prints , arXiv:2402.12115 (2024), arXiv:2402.12115 [cond-mat.str-el].
- ⁶⁹ Rhea Hoyer, Rodrigo Jaeschke-Ubierno, Kyo-Hoon Ahn, Libor Šmejkal, and Alexander Mook, “Spontaneous Crystal Thermal Hall Effect in Insulating Altermagnets,” arXiv e-prints , arXiv:2405.05090 (2024), arXiv:2405.05090 [cond-mat.mes-hall].
- ⁷⁰ Yu-Li Lee, “Magnetic impurities in an altermagnetic metal,” arXiv e-prints , arXiv:2312.15733 (2023), arXiv:2312.15733 [cond-mat.str-el].
- ⁷¹ Morten Amundsen, Arne Brataas, and Jacob Linder, “RKKY interaction in Rashba altermagnets,” arXiv e-prints , arXiv:2405.06736 (2024), arXiv:2405.06736 [cond-mat.mes-hall].
- ⁷² Rafael M. Fernandes, Vanuildo S. de Carvalho, Turan Birol, and Rodrigo G. Pereira, “Topological transition from nodal to nodeless Zeeman splitting in altermagnets,” *Phys. Rev. B* **109**, 024404 (2024).
- ⁷³ Daniil S. Antonenko, Rafael M. Fernandes, and Jorn W. F. Venderbos, “Mirror Chern Bands and Weyl Nodal Loops in Altermagnets,” arXiv e-prints , arXiv:2402.10201 (2024), arXiv:2402.10201 [cond-mat.mes-hall].
- ⁷⁴ Sayed Ali Akbar Ghorashi, Taylor L. Hughes, and Jennifer Cano, “Altermagnetic Routes to Majorana Modes in Zero Net Magnetization,” arXiv e-prints , arXiv:2306.09413 (2023), arXiv:2306.09413 [cond-mat.mes-hall].
- ⁷⁵ Yu-Xuan Li and Cheng-Cheng Liu, “Majorana corner modes and tunable patterns in an altermagnet heterostructure,” *Phys. Rev. B* **108**, 205410 (2023).
- ⁷⁶ Yu-Xuan Li, Yichen Liu, and Cheng-Cheng Liu, “Creation and manipulation of higher-order topological states by altermagnets,” *Phys. Rev. B* **109**, L201109 (2024).
- ⁷⁷ Yu-Xuan Li, “Realizing tunable higher-order topological superconductors with altermagnets,” *Phys. Rev. B* **109**, 224502 (2024).
- ⁷⁸ Motohiko Ezawa, “Detecting the Néel vector of altermagnet by attaching a topological insulator and crystalline valley-

- edge insulator,” arXiv e-prints , arXiv:2403.09150 (2024), arXiv:2403.09150 [cond-mat.mes-hall].
- ⁷⁹ Jeffrey C. Y. Teo and C. L. Kane, “Topological defects and gapless modes in insulators and superconductors,” *Phys. Rev. B* **82**, 115120 (2010).
- ⁸⁰ Ching-Kai Chiu, Jeffrey C. Y. Teo, Andreas P. Schnyder, and Shinsei Ryu, “Classification of topological quantum matter with symmetries,” *Rev. Mod. Phys.* **88**, 035005 (2016).
- ⁸¹ Shunyu Yao, Zhongbo Yan, and Zhong Wang, “Topological invariants of floquet systems: General formulation, special properties, and floquet topological defects,” *Phys. Rev. B* **96**, 195303 (2017).
- ⁸² N. D. Mermin, “The topological theory of defects in ordered media,” *Rev. Mod. Phys.* **51**, 591–648 (1979).
- ⁸³ M. Kleman and J. Friedel, “Disclinations, dislocations, and continuous defects: A reappraisal,” *Rev. Mod. Phys.* **80**, 61–115 (2008).
- ⁸⁴ Jeffrey C.Y. Teo and Taylor L. Hughes, “Topological defects in symmetry-protected topological phases,” *Annual Review of Condensed Matter Physics* **8**, 211–237 (2017).
- ⁸⁵ Zhi-Kang Lin, Qiang Wang, Yang Liu, Haoran Xue, Baile Zhang, Yidong Chong, and Jian-Hua Jiang, “Topological phenomena at defects in acoustic, photonic and solid-state lattices,” *Nature Reviews Physics* **5**, 483–495 (2023).
- ⁸⁶ Daichi Asahi and Naoto Nagaosa, “Topological indices, defects, and Majorana fermions in chiral superconductors,” *Phys. Rev. B* **86**, 100504 (2012).
- ⁸⁷ A. Bühler, N. Lang, C. V. Kraus, G. Möller, S. D. Huber, and H. P. Büchler, “Majorana modes and p-wave superfluids for fermionic atoms in optical lattices,” *Nature Communications* **5**, 4504 (2014).
- ⁸⁸ Taylor L. Hughes, Hong Yao, and Xiao-Liang Qi, “Majorana zero modes in dislocations of Sr_2RuO_4 ,” *Phys. Rev. B* **90**, 235123 (2014).
- ⁸⁹ Robert-Jan Slager, Andrej Mesaros, Vladimir Juričić, and Jan Zaanen, “Interplay between electronic topology and crystal symmetry: Dislocation-line modes in topological band insulators,” *Phys. Rev. B* **90**, 241403 (2014).
- ⁹⁰ Fernando de Juan, Andreas Rüegg, and Dung-Hai Lee, “Bulk-defect correspondence in particle-hole symmetric insulators and semimetals,” *Phys. Rev. B* **89**, 161117 (2014).
- ⁹¹ Guido van Miert and Carmine Ortix, “Dislocation charges reveal two-dimensional topological crystalline invariants,” *Phys. Rev. B* **97**, 201111 (2018).
- ⁹² Bitan Roy and Vladimir Juričić, “Dislocation as a bulk probe of higher-order topological insulators,” *Phys. Rev. Res.* **3**, 033107 (2021).
- ⁹³ Rodrigo Soto-Garrido, Enrique Muñoz, and Vladimir Juričić, “Dislocation defect as a bulk probe of monopole charge of multi-weyl semimetals,” *Phys. Rev. Res.* **2**, 012043 (2020).
- ⁹⁴ Frank Schindler, Stepan S. Tsirkin, Titus Neupert, B. Andrei Bernevig, and Benjamin J. Wieder, “Topological zero-dimensional defect and flux states in three-dimensional insulators,” *Nature Communications* **13**, 5791 (2022).
- ⁹⁵ Lun-Hui Hu and Rui-Xing Zhang, “Dislocation Majorana bound states in iron-based superconductors,” *Nature Communications* **15**, 2337 (2024).
- ⁹⁶ Ying Ran, Yi Zhang, and Ashvin Vishwanath, “One-dimensional topologically protected modes in topological insulators with lattice dislocations,” *Nature Physics* **5**, 298–303 (2009).
- ⁹⁷ Liang Fu and C. L. Kane, “Topological insulators with inversion symmetry,” *Phys. Rev. B* **76**, 045302 (2007).
- ⁹⁸ Ying Ran, “Weak indices and dislocations in general topological band structures,” arXiv e-prints , arXiv:1006.5454 (2010), arXiv:1006.5454 [cond-mat.str-el].
- ⁹⁹ Vladimir Juričić, Andrej Mesaros, Robert-Jan Slager, and Jan Zaanen, “Universal Probes of Two-Dimensional Topological Insulators: Dislocation and π Flux,” *Phys. Rev. Lett.* **108**, 106403 (2012).
- ¹⁰⁰ Xiao-Liang Qi, Yong-Shi Wu, and Shou-Cheng Zhang, “Topological quantization of the spin Hall effect in two-dimensional paramagnetic semiconductors,” *Phys. Rev. B* **74**, 085308 (2006).
- ¹⁰¹ David Aasen, Michael Hell, Ryan V. Mishmash, Andrew Higginbotham, Jeroen Danon, Martin Leijnse, Thomas S. Jespersen, Joshua A. Folk, Charles M. Marcus, Karsten Flensberg, and Jason Alicea, “Milestones Toward Majorana-Based Quantum Computing,” *Phys. Rev. X* **6**, 031016 (2016).
- ¹⁰² Jay D. Sau, Roman M. Lutchyn, Sumanta Tewari, and S. Das Sarma, “Generic New Platform for Topological Quantum Computation Using Semiconductor Heterostructures,” *Phys. Rev. Lett.* **104**, 040502 (2010).